Exhibit 14
Part 2

where $\mathscr{E}_m$ is the maximum field that exists at $x = 0$ and is given by

$$|\mathscr{E}_m| = \frac{qN_D x_n}{\epsilon_s} = \frac{qN_A x_p}{\epsilon_s}. \tag{12}$$

Integrating Eq. 10 once again, Fig. 10c, gives the potential distribution $V(x)$ and the built-in potential V_{bi}:

$$V(x) = \mathscr{E}_m\left(x - \frac{x^2}{2W}\right) \tag{13}$$

$$V_{bi} = \tfrac{1}{2}\mathscr{E}_m W \equiv \tfrac{1}{2}\mathscr{E}_m(x_n + x_p) \tag{14}$$

where W is the total depletion width. Eliminating $\mathscr{E}_m$ from Eqs. 12 and 14 yields

$$W = \sqrt{\frac{2\epsilon_s}{q}\left(\frac{N_A + N_D}{N_A N_D}\right) V_{bi}} \tag{15}$$

for a two-sided abrupt junction. For a one-sided abrupt junction, Eq. 15 reduces to

$$W = \sqrt{\frac{2\epsilon_s V_{bi}}{qN_B}} \tag{15a}$$

where $N_B = N_D$ or N_A depending on whether $N_A \gg N_D$ or vice versa.

A more accurate result for the depletion-layer width can be obtained from Eq. 10 by considering the majority-carrier contribution in addition to the impurity concentration, that is, $\rho \approx -q[N_A - p(x)]$ on the p side and $\rho \approx q[N_D - n(x)]$ on the n side. The depletion width is essentially the same as given by Eq. 15, except that V_{bi} is replaced by $(V_{bi} - 2kT/q)$. The correction factor $2kT/q$ comes about because of the two majority-carrier distribution tails[26] (electrons in n side and holes in p side, as shown by the dashed lines in Fig. 10*a*). Each contributes a correction factor kT/q. The correction is simply the dipole moment of the "error" distribution—the true carrier distribution minus the abrupt distribution. The depletion-layer width at thermal equilibrium for a one-sided abrupt junction becomes

$$W = \sqrt{\frac{2\epsilon_s}{qN_B}(V_{bi} - 2kT/q)}$$

$$= L_D\sqrt{2(\beta V_{bi} - 2)} \tag{16}$$

where $\beta = q/kT$ and L_D is the Debye length, which is a characteristic length for semiconductors. The Debye length is defined as

$$L_D \equiv \sqrt{\frac{\epsilon_s kT}{q^2 N_B}} = \sqrt{\frac{\epsilon_s}{qN_B\beta}}. \tag{17}$$

At thermal equilibrium the depletion-layer widths of abrupt junctions are about $6L_D$ for Ge, $8L_D$ for Si, and $10L_D$ for GaAs. The Debye length as a function of doping density is shown in Fig. 12 for silicon at room tem-

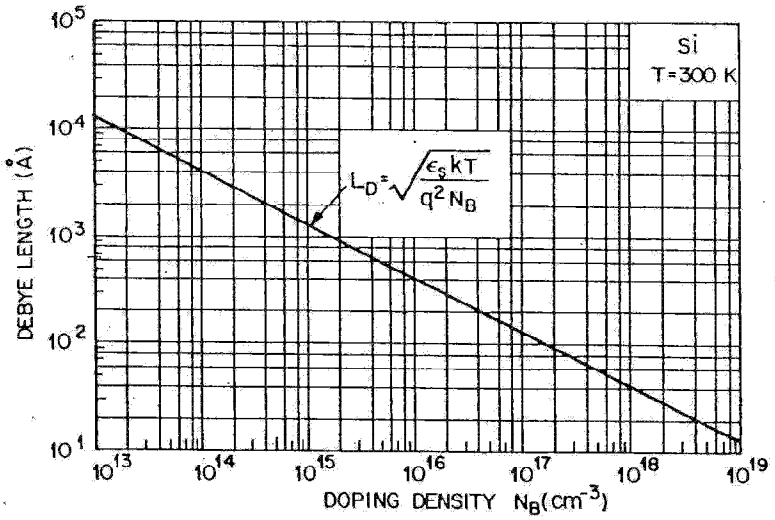

Fig. 12 Debye length in Si as a function of doping density.

perature. For a doping density of $10^{16}\,cm^{-3}$, the Debye length is 400 Å; for other dopings, L_D will vary as $1/\sqrt{N_B}$, that is, a reduction by a factor of 3.16 per decade.

The values of W as a function of the doping concentration for one-sided abrupt junctions in silicon are shown in Fig. 13 (dashed line for zero bias). When a voltage V is applied to the junction, the total electrostatic potential

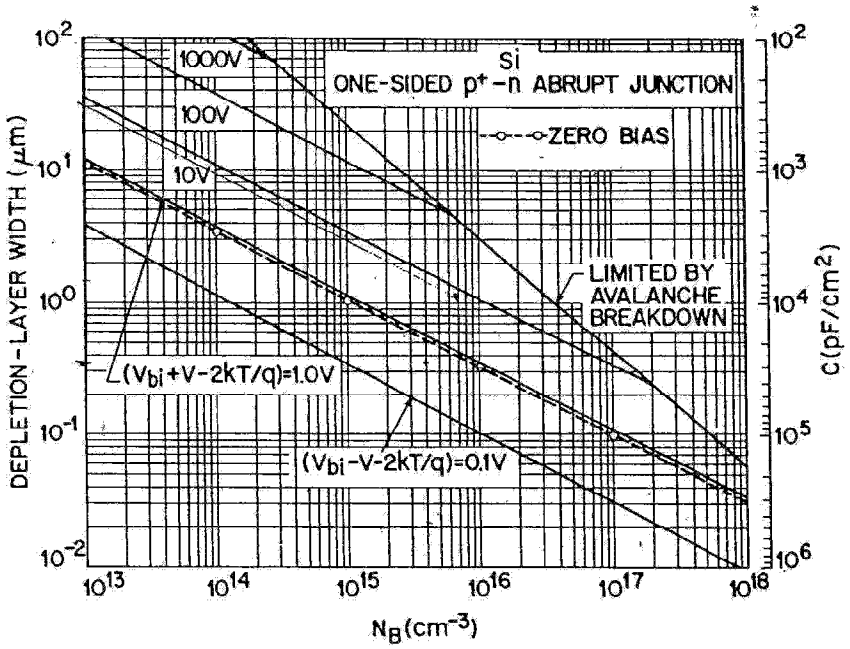

Fig. 13 Depletion-layer width and depletion-layer capacitance per unit area as a function of doping for one-sided abrupt junction in Si. The dashed line is for the case of zero-bias voltage.

variation across the junction is given by $(V_{bi} + V)$ for reverse bias (positive voltage on n region with respect to p region) and by $(V_{bi} - V)$ for forward bias. Substituting these voltage values in Eq. 16 yields the depletion-layer width as a function of the applied voltage. The results for one-sided abrupt junctions in silicon are shown in Fig. 13. The values below the zero-bias line (dashed line) are for the forward-biased condition; and above, for the reverse-biased condition.

These results can also be used for GaAs since both Si and GaAs have approximately the same static dielectric constants. To obtain the depletion-layer width for Ge, one must multiply the results of Si by the factor

$$\sqrt{\epsilon_s(\text{Ge})/\epsilon_s(\text{Si})} = 1.16.$$

The simple model above can give adequate predictions for most abrupt p-n junctions. However, for strongly asymmetrical junctions or for devices with ultrashallow junction depths, numerical analysis may be needed for accurate results.[27] The electric field region near the junction cannot be confined to the shaded region as shown in the left diagram of Fig. 8*a*, because any doping gradient creates a field (refer to Eq. 5). The strong doping gradient clearly extends well outside the shaded region. Figure 14 shows an example of a diffused junction 0.25 μm deep with $C_s = 2 \times 10^{20}\ \text{cm}^{-3}$, an erfc profile, and $N_A = 5 \times 10^{15}\ \text{cm}^{-3}$. The equilibrium energy-band diagram is shown in Fig. 14*a*. Note that the conduction band goes below the Fermi level near the surface due to high surface concentration. The electric field profile is shown in Fig. 14*b*. There are several important differences in the field profiles between the simple model and the numerical results. First, the actual field region on the diffused side is five times wider than it is in the simple model. Second, the electric field is always larger than 10^4 V/cm throughout the surface region, so that transport processes can be strongly affected. The space-charge distribution (assuming negligible surface-charge effects) is shown in Fig. 14*c*. Apparently, the space charge on the diffused side is considerably widened beyond the depletion-layer width $-x_p$ in the simple model.

Depletion-Layer Capacitance The depletion-layer capacitance per unit area is defined as $C \equiv dQ_c/dV$, where dQ_c is the incremental increase in charge per unit area upon an incremental change of the applied voltage dV.

For one-sided abrupt junctions, the capacitance per unit area is given by

$$C \equiv \frac{dQ_c}{dV} = \frac{d(qN_BW)}{d[(qN_B/2\epsilon_s)W^2]} = \frac{\epsilon_s}{W} = \sqrt{\frac{q\epsilon_s N_B}{2}}\,(V_{bi} \pm V - 2kT/q)^{-1/2}$$

$$= \frac{\epsilon_s}{\sqrt{2}L_D}\,(\beta V_{bi} \pm \beta V - 2)^{-1/2} \qquad \text{F/cm}^2 \tag{18}$$

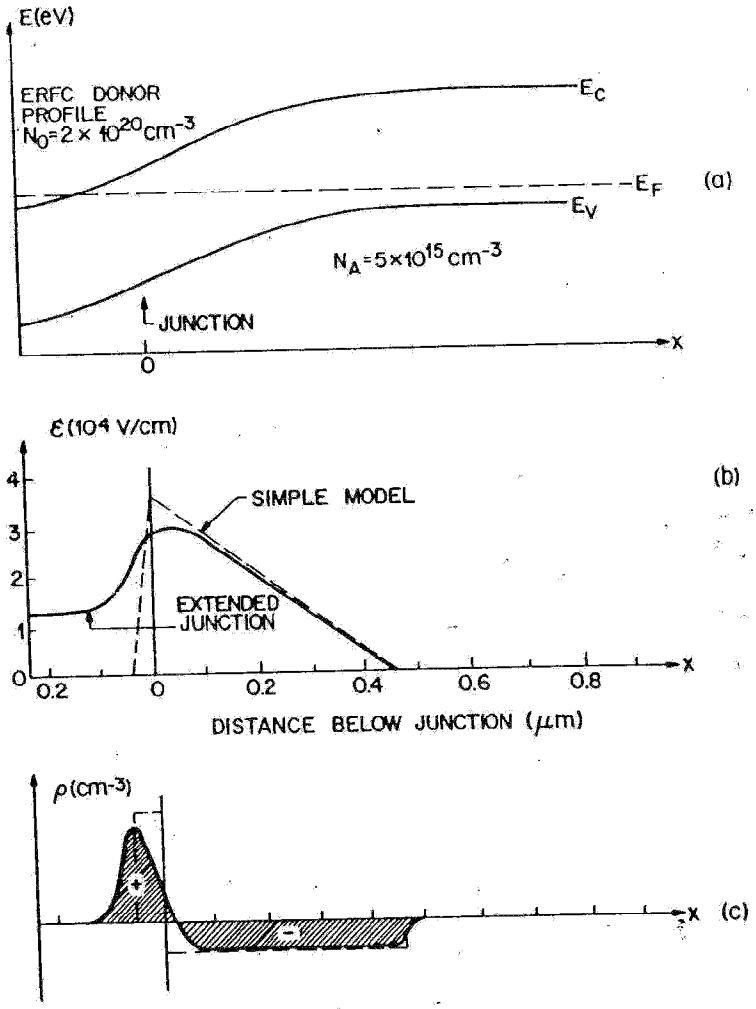

Fig. 14 Strongly asymmetrical junction. (*a*) Energy-band diagram. (*b*) Electric field distribution. (c) Space-charge distribution. (After Redfield, Ref. 27.)

or

$$\frac{1}{C^2}=\frac{2L_D^2}{\epsilon_s^2}(\beta V_{bi}\pm\beta V-2) \tag{18a}$$

$$\frac{d(1/C^2)}{dV}\cong\frac{2L_D^2\beta}{\epsilon_s^2}=\frac{2}{q\epsilon_s N_B} \tag{18b}$$

where the ± signs are for the reverse- and forward-bias conditions, respectively. It is clear from Eq. 18a that by plotting $1/C^2$ versus V, a straight line should result for a one-sided abrupt junction. The slope gives the impurity concentration of the substrate (N_B), and the intercept (at $1/C^2=0$) gives ($V_{bi}-2kT/q$). The results of the capacitance are also shown in Fig. 13. Note that, for the forward bias, a diffusion capacitance exists in addition to the depletion capacitance mentioned previously. The diffusion capacitance is discussed in Section 3.4.

Equation 18b holds for more general distributions than just for the abrupt p^+-n junction. For a general distribution we have

$$\frac{d(1/C^2)}{dV} = \frac{2}{q\epsilon_s N(W)} \tag{18c}$$

and

$$W = \frac{\epsilon_s}{C(V)} \tag{18d}$$

where $N(W)$ is the doping density at $x = W$.

Note also that the capacitance–voltage data are insensitive to changes in the doping profiles that occur in a distance less than a Debye length of the highly doped side, and so the doping profiles determined by the C–V method should be expected to provide a spatial resolution of only the order of a Debye length.[28]

2.3.2 Linearly Graded Junction

Consider the thermal equilibrium case first. The impurity distribution for linearly graded junctions is shown in Fig. 15*a*. The Poisson equation for this case is

$$-\frac{\partial^2 V}{\partial x^2} \equiv \frac{\partial \mathscr{E}}{\partial x} = \frac{\rho(x)}{\epsilon_s} = \frac{q}{\epsilon_s}(p - n + ax) \approx \frac{q}{\epsilon_s} ax \qquad -\frac{W}{2} \le x \le \frac{W}{2} \tag{19}$$

where a is the impurity gradient in cm^{-4}. By integrating Eq. 19 once, we obtain the field distribution shown in Fig. 15*b*:

$$\mathscr{E}(x) = -\frac{qa}{\epsilon_s}\frac{(W/2)^2 - x^2}{2} \tag{20}$$

with the maximum field $\mathscr{E}_m$ at $x = 0$,

$$|\mathscr{E}_m| = \frac{qaW^2}{8\epsilon_s}. \tag{20a}$$

Integrating Eq. 19 once again gives the built-in potential shown in Fig. 15*c*:

$$V_{bi} = \frac{qaW^3}{12\epsilon_s} \tag{21}$$

or

$$W = \left(\frac{12\epsilon_s V_{bi}}{qa}\right)^{1/3}. \tag{21a}$$

Since the values of the impurity concentrations at the edges of the depletion region ($-W/2$ and $W/2$) are equal to $aW/2$, the built-in potential for linearly graded junctions can be approximated by an expression similar

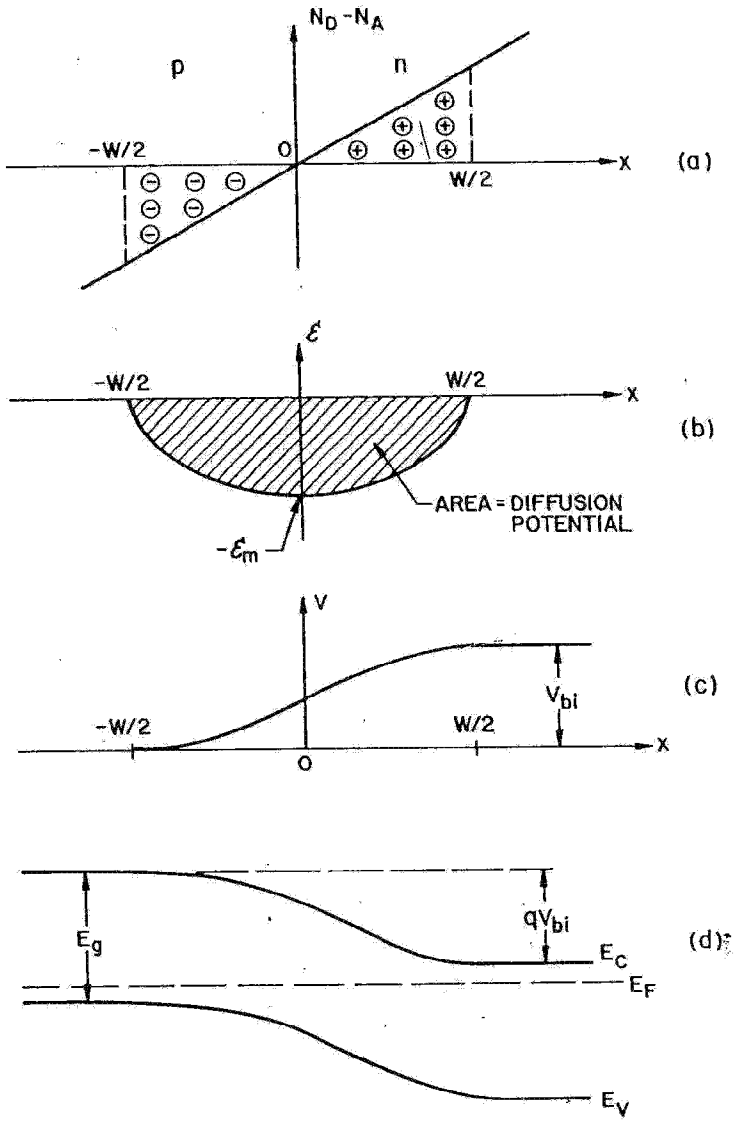

Fig. 15 Linearly graded junction in thermal equilibrium. (*a*) Space-charge distribution. (*b*) Electric field distribution. (*c*) Potential variation with distance. (*d*) Energy-band diagram.

to Eq. 7:

$$V_{bi} \simeq \frac{kT}{q} \ln\left[\frac{(aW/2)(aW/2)}{n_i^2}\right] = \frac{kT}{q} \ln\left(\frac{aW}{2n_i}\right)^2. \tag{22}$$

The depletion-layer capacitance for a linearly graded junction is given by

$$C \equiv \frac{dQ_c}{dV} = \frac{d(qaW^2/8)}{d(qaW^3/12\epsilon_s)} = \frac{\epsilon_s}{W} = \left[\frac{qa\epsilon_s^2}{12(V_{bi} \pm V)}\right]^{1/3} \quad \text{F/cm}^2 \tag{23}$$

where the signs + and − are for the reverse and forward bias, respectively. Based on an accurate numerical technique,[29] the depletion-layer capaci-

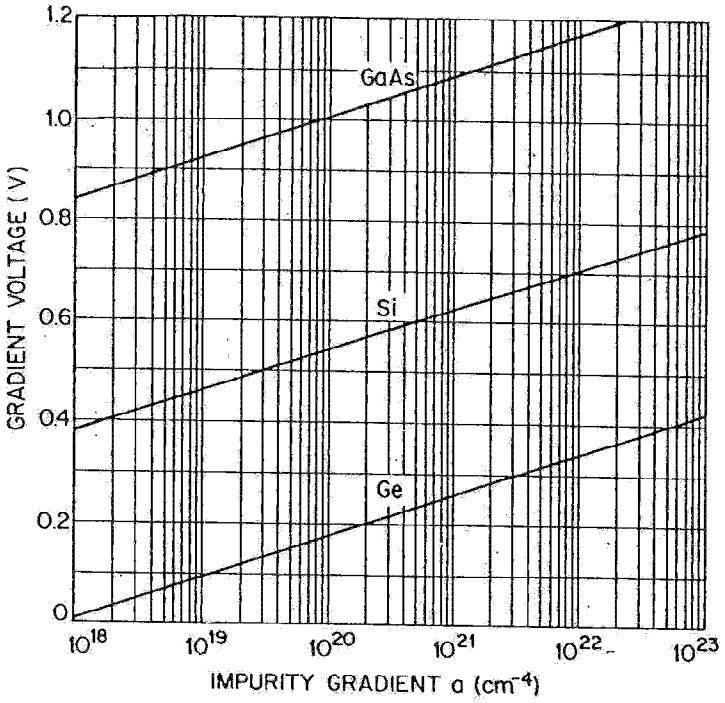

Fig. 16 Gradient voltage for linearly graded junctions in Ge, Si, and GaAs.

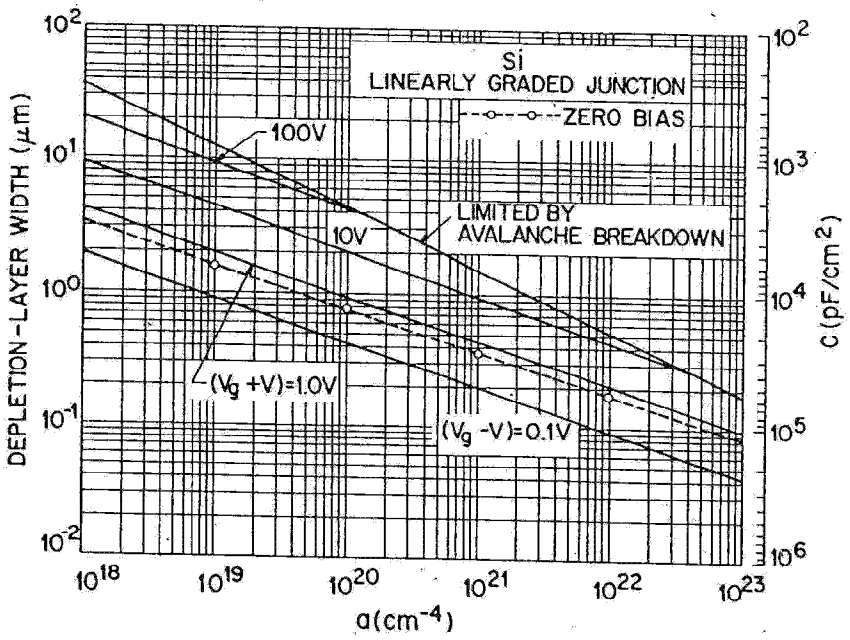

Fig. 17 Depletion-layer width and depletion-layer capacitance per unit area as a function of impurity gradient for linearly graded junctions in Si. The dashed line is for the case of zero-bias voltage.

tance is given by an expression identical to Eq. 23 except that the V_{bi} is replaced by a "gradient voltage" V_g:

$$V_g = \frac{2}{3}\frac{kT}{q}\ln\left[\frac{a^2\epsilon_s kT/q}{8qn_i^3}\right]. \tag{24}$$

The gradient voltages for Ge, Si, and GaAs as a function of impurity gradient are shown in Fig. 16. These voltages are smaller than the V_{bi} calculated from Eq. 22 by more than 100 mV. The depletion-layer width and the corresponding capacitance for silicon are plotted in Fig. 17 as a function of impurity gradient.

2.4 CURRENT–VOLTAGE CHARACTERISTICS

2.4.1 Ideal Case—Shockley Equation[1]

The ideal current–voltage characteristics are based on the following four assumptions: (1) the abrupt depletion-layer approximation; that is, the built-in potential and applied voltages, are supported by a dipole layer with abrupt boundaries, and outside the boundaries the semiconductor is assumed to be neutral; (2) the Boltzmann approximation; that is, throughout the depletion layer, the Boltzmann relations similar to Eqs. 33 and 37 of Chapter 1 are valid; (3) the low injection assumption; that is, the injected minority carrier densities are small compared with the majority-carrier densities; and (4) no generation current exists in the depletion layer, and the electron and hole currents are constant through the depletion layer.

We first consider the Boltzmann relation. At thermal equilibrium this relation is given by

$$n = n_i \exp\left(\frac{E_F - E_i}{kT}\right) \equiv n_i \exp\left[\frac{q(\psi - \phi)}{kT}\right] \tag{25a}$$

$$p = n_i \exp\left(\frac{E_i - E_F}{kT}\right) \equiv n_i \exp\left[\frac{q(\phi - \psi)}{kT}\right] \tag{25b}$$

where ψ and ϕ are the potentials corresponding to the intrinsic level and the Fermi level, respectively (or $\psi \equiv -E_i/q$, $\phi \equiv -E_F/q$). Obviously, at thermal equilibrium, the pn product from Eqs. 25a and 25b is equal to n_i^2. When voltage is applied, the minority-carrier densities on both sides of a junction are changed, and the pn product is no longer given by n_i^2. We shall now define the imrefs as follows:

$$n \equiv n_i \exp\left[\frac{q(\psi - \phi_n)}{kT}\right] \tag{26a}$$

$$p = n_i \exp\left[\frac{q(\phi_p - \psi)}{kT}\right] \tag{26b}$$

where ϕ_n and ϕ_p are the imrefs or quasi-Fermi levels for electrons and holes, respectively. From Eqs. 26a and 26b we obtain

$$\phi_n \equiv \psi - \frac{kT}{q} \ln\left(\frac{n}{n_i}\right) \tag{27a}$$

$$\phi_p \equiv \psi + \frac{kT}{q} \ln\left(\frac{p}{n_i}\right). \tag{27b}$$

The pn product becomes

$$pn = n_i^2 \exp\left[\frac{q(\phi_p - \phi_n)}{kT}\right]. \tag{28}$$

For a forward bias, $(\phi_p - \phi_n) > 0$ and $pn > n_i^2$; on the other hand, for a reversed bias, $(\phi_p - \phi_n) < 0$ and $pn < n_i^2$.

From Eq. 93 of Chapter 1, Eq. 26a, and from the fact that $\mathscr{E} \equiv -\nabla\psi$, we obtain

$$\mathbf{J}_n = q\mu_n\left(n\mathscr{E} + \frac{kT}{q}\nabla n\right) = q\mu_n n(-\nabla\psi) + q\mu_n \frac{kT}{q}\left[\frac{qn}{kT}(\nabla\psi - \nabla\phi_n)\right]$$
$$= -q\mu_n n \nabla\phi_n. \tag{29}$$

Similarly, we obtain

$$\mathbf{J}_p = -q\mu_p p \nabla\phi_p. \tag{30}$$

Thus the electron and hole current densities are proportional to the gradients of the electron and hole imref, respectively. If $\phi_n = \phi_p = \phi =$ constant (at thermal equilibrium), then $\mathbf{J}_n = \mathbf{J}_p = 0$.

The idealized potential distributions and the carrier concentrations in a p-n junction under forward-bias and reverse-bias conditions are shown in Fig. 18. The variations of ϕ_n and ϕ_p with distance are related to the carrier concentrations as given in Eq. 27. Since the electron density n varies in the junction from the n side to the p side by many orders of magnitude, while the electron current J_n is almost constant, it follows that ϕ_n must also be almost constant over the depletion layer. The electrostatic potential difference across the junction is given by

$$V = \phi_p - \phi_n. \tag{31}$$

Equations 28 and 31 can be combined to give the electron density at the boundary of the depletion-layer region on the p side ($x = -x_p$):

$$n_p = \frac{n_i^2}{p_p} \exp\left(\frac{qV}{kT}\right) = n_{po} \exp\left(\frac{qV}{kT}\right) \tag{32}$$

where n_{po} is the equilibrium electron density on the p side. Similarly,

$$p_n = p_{no} \exp\left(\frac{qV}{kT}\right) \tag{33}$$

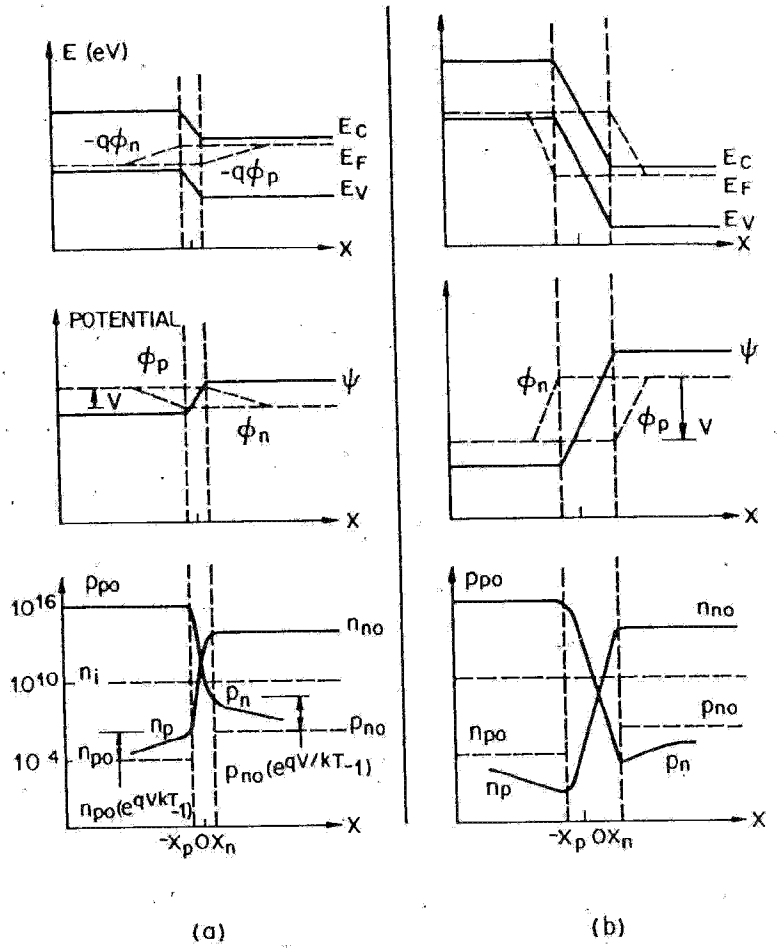

Fig. 18 Energy-band diagram; intrinsic Fermi level (ψ); quasi-Fermi level, also referred to as imref (ϕ_n for electrons, ϕ_p for holes); and carrier distributions under (a) forward-biased conditions and (b) reverse-biased conditions. (After Shockley, Ref. 1.)

at $x = x_n$ for the n-type boundary. The preceding equations are the most important boundary conditions for the ideal current–voltage equation.

From the continuity equations we obtain for the steady state:

$$-U + \mu_n \mathscr{E} \frac{\partial n_n}{\partial x} + \mu_n n_n \frac{\partial \mathscr{E}}{\partial x} + D_n \frac{\partial^2 n_n}{\partial x^2} = 0 \tag{34a}$$

$$-U - \mu_p \mathscr{E} \frac{\partial p_n}{\partial x} - \mu_p p_n \frac{\partial \mathscr{E}}{\partial x} + D_p \frac{\partial^2 p_n}{\partial x^2} = 0. \tag{34b}$$

In these equations, U is the net recombination rate. The charge neutrality holds approximately, so that $(n_n - n_{no}) \approx (p_n - p_{no})$. Multiplying Eq. 34a by $\mu_p p_n$ and Eq. 34b by $\mu_n n_n$, and combining with the Einstein relation, $D = (kT/q)\mu$, we have

$$-\frac{p_n - p_{no}}{\tau_a} + D_a \frac{\partial^2 p_n}{\partial x^2} - \frac{n_n - p_n}{n_n/\mu_p + p_n/\mu_n} \frac{\mathscr{E} \partial p_n}{\partial x} = 0 \tag{35}$$

where

$$D_a = \frac{n_n + p_n}{n_n/D_p + p_n/D_n} = \text{ambipolar diffusion coefficient} \tag{36}$$

$$\tau_a = \frac{p_n - p_{no}}{U} = \frac{n_n - n_{no}}{U} = \text{ambipolar lifetime.} \tag{37}$$

From the low-injection assumption (e.g., $p_n \ll n_n \approx n_{no}$ in the n-type semiconductor), Eq. 35 reduces to

$$-\frac{p_n - p_{no}}{\tau_p} - \mu_p \mathscr{E} \frac{\partial p_n}{\partial x} + D_p \frac{\partial^2 p_n}{\partial x^2} = 0 \tag{38}$$

which is Eq. 34b except that the term $\mu_p p_n \partial \mathscr{E}/\partial x$ is missing; under the low-injection assumption, this term is of the same order as the neglected terms.

In the neutral region where there is no electric field, Eq. 38 reduces further to

$$\frac{\partial^2 p_n}{\partial x^2} - \frac{p_n - p_{no}}{D_p \tau_p} = 0. \tag{39}$$

The solution of Eq. 39 with the boundary condition Eq. 33 and $p_n(x = \infty) = p_{no}$ gives

$$p_n - p_{no} = p_{no}(e^{qV/kT} - 1)e^{-(x-x_n)/L_p} \tag{40}$$

where

$$L_p \equiv \sqrt{D_p \tau_p}. \tag{41}$$

And at $x = x_n$,

$$J_p = -qD_p \left.\frac{\partial p_n}{\partial x}\right|_{x_n} = \frac{qD_p p_{no}}{L_p}(e^{qV/kT} - 1). \tag{42}$$

Similarly, we obtain for the p side

$$J_n = qD_n \left.\frac{\partial n_p}{\partial x}\right|_{-x_p} = \frac{qD_n n_{po}}{L_n}(e^{qV/kT} - 1). \tag{43}$$

The minority-carrier densities and the current densities for the forward-bias and reverse-bias condition are shown in Fig. 19.

The total current is given by the sum of Eqs. 42 and 43:

$$J = J_p + J_n = J_s(e^{qV/kT} - 1), \tag{44}$$

$$J_s \equiv \frac{qD_p p_{no}}{L_p} + \frac{qD_n n_{po}}{L_n}. \tag{45}$$

Equation 45 is the celebrated Shockley equation,[1] which is the ideal diode law. The ideal current–voltage relation is shown in Fig. 20*a* and *b* in the linear and semilog plots, respectively. In the forward direction (positive

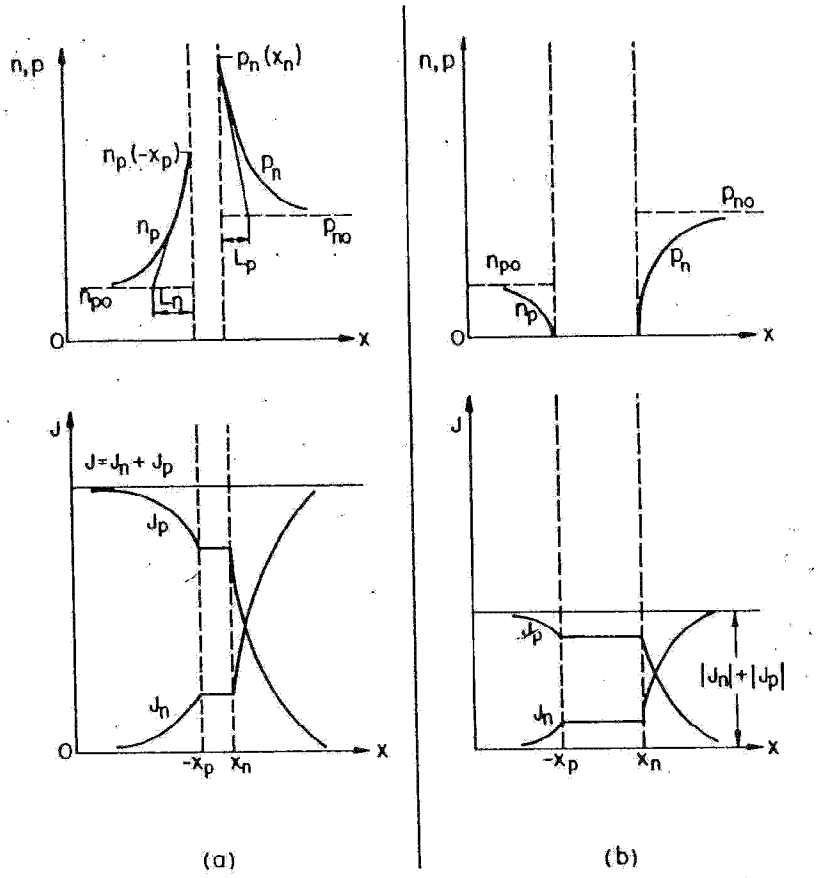

Fig. 19 Carrier distributions and current densities (both linear plots) for (*a*) forward-biased conditions and (*b*) reverse-biased conditions. (After Shockley, Ref. 1.)

bias on p) for $V > 3kT/q$, the rate of rise is constant, Fig. 20*b*; at 300 K for every decade change of current, the voltage changes by 59.5 mV ($= 2.3kT/q$). In the reverse direction, the current density saturates at $-J_s$.

We shall now briefly consider the temperature effect on the saturation current density J_s. We shall consider only the first term in Eq. 45, since the second term will behave similarly to the first one. For the one-sided p^+n abrupt junction (with donor concentration N_D), $p_{no} \gg n_{po}$, the second term also can be neglected. The quantities D_p, p_{no}, and L_p ($\equiv \sqrt{D_p \tau_p}$) are all temperature-dependent. If D_p/τ_p is proportional to T^γ, where γ is a constant, then

$$J_s \simeq \frac{qD_p p_{no}}{L_p} \simeq q\sqrt{\frac{D_p}{\tau_p}}\frac{n_i^2}{N_D}$$
$$\sim \left[T^3 \exp\left(-\frac{E_g}{kT}\right)\right] T^{\gamma/2} = T^{(3+\gamma/2)} \exp\left(-\frac{E_g}{kT}\right). \tag{46}$$

The temperature dependence of the term $T^{(3+\gamma/2)}$ is not important compared with the exponential term. The slope of a plot J_s versus $1/T$ is determined by the energy gap E_g. It is expected that in the reverse direction, where

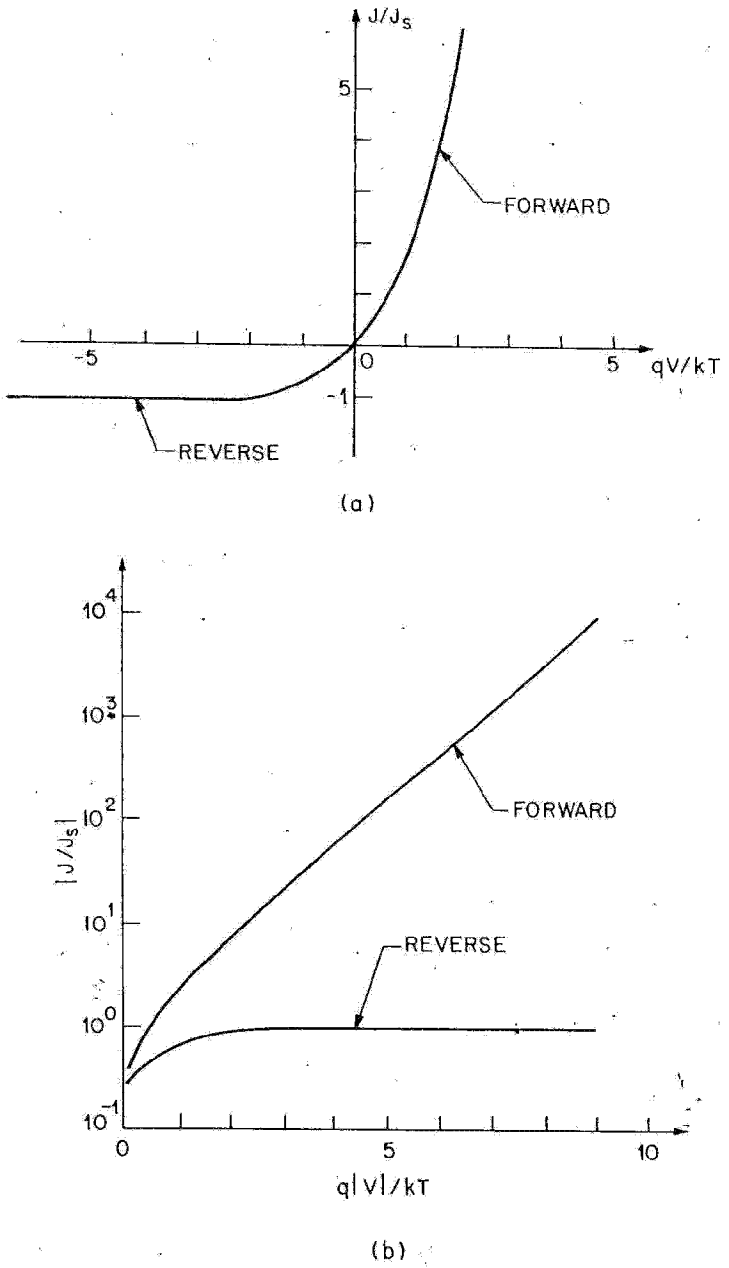

Fig. 20 Ideal current–voltage characteristics. (a) Linear plot. (*b*) Semilog plot.

$|J_R| \sim J_s$, the current will increase approximately as $e^{-E_g/kT}$ with temperature; and in the forward direction, where $J_F \sim J_s e^{qV/kT}$, the current will increase approximately as $\exp[-(E_g - qV)/kT]$.

2.4.2 Generation–Recombination Process[2]

The Shockley equation adequately predicts the current–voltage characteristics of germanium p-n junctions at low current densities. For Si and

GaAs p-n junctions, however, the ideal equation can give only qualitative agreement. The departures from the ideal are mainly due to: (1) the surface effect, (2) the generation and recombination of carriers in the depletion layer, (3) the tunneling of carriers between states in the bandgap, (4) the high-injection condition that may occur even at relatively small forward bias, and (5) the series resistance effect. In addition, under sufficiently larger field in the reverse direction, the junction will break down (as a result, for example, of avalanche multiplication). The junction breakdown will be discussed in Section 2.5.

The surface effects on p-n junctions are due primarily to ionic charges on or outside the semiconductor surface that induce image charges in the semiconductor and thereby cause the formation of the so-called surface channels or surface depletion-layer regions. Once a channel is formed, it modifies the junction depletion region and gives rise to surface leakage current. The details of the surface effect are discussed in Chapters 7 and 8. For Si planar p-n junctions, the surface leakage current is generally much smaller than the generation current in the depletion region.

Consider first the generation current under the reverse-bias condition. Because of the reduction in carrier concentration under reverse bias ($pn \ll n_i^2$), the dominant recombination–generation processes as discussed in Chapter 1 are those of emission. The rate of generation of electron–hole pairs can be obtained from Eq. 58 of Chapter 1 with the condition $p < n_i$ and $n < n_i$:

$$U = -\left[\frac{\sigma_p \sigma_n v_{th} N_t}{\sigma_n \exp\left(\dfrac{E_t - E_i}{kT}\right) + \sigma_p \exp\left(\dfrac{E_i - E_t}{kT}\right)}\right] n_i \equiv -\frac{n_i}{\tau_e} \tag{47}$$

where τ_e is the effective lifetime and is defined as the reciprocal of the expression in brackets. The current due to the generation in the depletion region is thus given by

$$J_{\text{gen}} = \int_0^W q|U|dx \simeq q|U|W = \frac{qn_iW}{\tau_e} \tag{48}$$

where W is the depletion-layer width. If the effective lifetime is a slowly varying function of temperature, the generation current will then have the same temperature dependence as n_i. At a given temperature, J_{gen} is proportional to the depletion-layer width, which, in turn, is dependent on the applied reverse bias. It is thus expected that

$$J_{\text{gen}} \sim (V_{bi} + V)^{1/2} \tag{49a}$$

for abrupt junctions, and

$$J_{\text{gen}} \sim (V_{bi} + V)^{1/3} \tag{49b}$$

for linearly graded junctions.

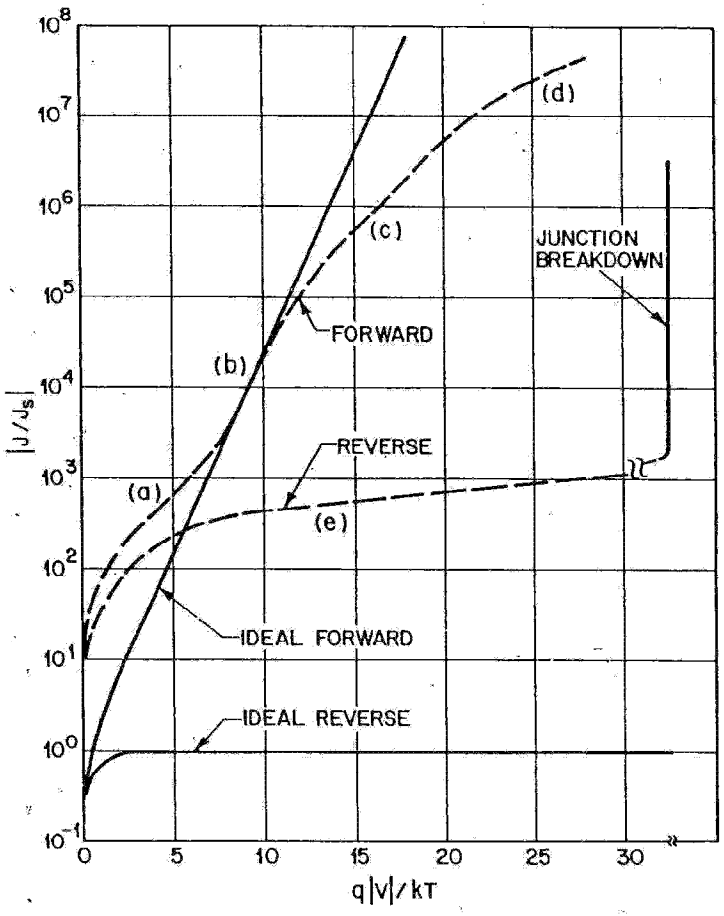

Fig. 21 Current–voltage characteristics of a practical Si diode. (*a*) Generation–recombination current region. (*b*) Diffusion current region. (*c*) High-injection region. (*d*) Series resistance effect. (e) Reverse leakage current due to generation–recombination and surface effects. (After Moll, Ref. 3.)

The total reverse current (for $p_{no} \gg n_{po}$ and $|V| > 3kT/q$) can be approximately given by the sum of the diffusion components in the neutral region and the generation current in the depletion region:

$$J_R = q\sqrt{\frac{D_p}{\tau_p}}\frac{n_i^2}{N_D} + \frac{qn_iW}{\tau_e}. \tag{50}$$

For semiconductors with large values of n_i (such as Ge), the diffusion component will dominate at room temperature and the reverse current will follow the Shockley equation; but if n_i is small (such as for Si), the generation current may dominate. A typical result[3] for Si is shown in Fig. 21, curve (e). At sufficiently high temperatures, however, the diffusion current will dominate.

At forward bias, where the major recombination–generation processes in the depletion region are the capture processes, we have a recombination current J_{rec} in addition to the diffusion current. Substituting Eq. 28 in Eq. 58

of Chapter 1 yields

$$U = \frac{\sigma_p \sigma_n v_{th} N_t n_i^2 (e^{qV/kT} - 1)}{\sigma_n \left[n + n_i \exp\left(\frac{E_t - E_i}{kT}\right)\right] + \sigma_p \left[p + n_i \exp\left(\frac{E_i - E_t}{kT}\right)\right]}. \tag{51}$$

Under the assumptions that $E_i = E_t$ and $\sigma_n = \sigma_p = \sigma$, Eq. 51 reduces to

$$U = \frac{\sigma v_{th} N_t n_i^2 (e^{qV/kT} - 1)}{n + p + 2n_i} \tag{52}$$

$$= \frac{\sigma v_{th} N_t n_i^2 (e^{qV/kT} - 1)}{n_i \left\{ \exp\left[\frac{q(\psi - \phi_n)}{kT}\right] + \exp\left[\frac{q(\phi_p - \psi)}{kT}\right] + 2 \right\}}. \tag{52a}$$

The maximum value of U exists in the depletion region where ψ is halfway between ϕ_p and ϕ_n, or $\psi = (\phi_n + \phi_p)/2$, and so the denominator of Eq. 52a becomes $2n_i[\exp(qV/2kT) + 1]$. We obtain for $V > kT/q$,

$$U \simeq \frac{1}{2} \sigma v_{th} N_t n_i \exp\left(\frac{qV}{2kT}\right) \tag{53}$$

and

$$J_{rec} = \int_0^W qU \, dx \approx \frac{qW}{2} \sigma v_{th} N_t n_i \exp\left(\frac{qV}{2kT}\right) \sim n_i N_t. \tag{54}$$

Similar to the generation current in reverse bias, the recombination current in forward bias is also proportional to n_i. The total forward current can be approximated by the sum of Eqs. 44 and 54 for $p_{no} \gg n_{po}$ and $V > kT/q$:

$$J_F = q \sqrt{\frac{D_p}{\tau_p}} \frac{n_i^2}{N_D} \exp\left(\frac{qV}{kT}\right) + \frac{qW}{2} \sigma v_{th} N_t n_i \exp\left(\frac{qV}{2kT}\right). \tag{55}$$

The experimental results in general can be represented by the empirical form,

$$J_F \sim \exp\left(\frac{qV}{nkT}\right) \tag{56}$$

where the factor n equals 2 when the recombination current dominates [Fig. 21, curve (a)] and n equals 1 when the diffusion current dominates [Fig. 21, curve (b)]. When both currents are comparable, n has a value between 1 and 2.

2.4.3 High-Injection Condition

At high current densities (under the forward-bias condition) such that the injected minority-carrier density is comparable with the majority concentration, both drift and diffusion current components must be considered. The individual conduction current densities can always be given by Eqs. 29